J Nanostruct 15(3): 983-996, Summer 2025

RESEARCH PAPER

Removal of Pb (II) Ions from Water by Adsorption on Sodium Alginate-g-poly (Acrylic acid-co-Itaconic acid)/Titanium Dioxide [SA-g-p(AA-IA)/ TiO_2] Hydrogel Nanocomposite

Mahmood Oudah Mutashar [1], ***Raad Farhan Shahad*** [2], ***Layth Sameer Jasim*** [3]*, ***Maryam Batool*** [4]

[1] *Ministry of Education General Directorate of Maysan Education, Misan, Iraq*

[2] *Department of Soil and Water Resources Sciences, University of Al-Qadisiyah, Al-Diwaniyah, Iraq*

[3] *Department of Chemistry, College of Education, University of Al-Qadisiyah, Diwaniyah, Iraq*

[4] *Department of Chemistry, University of Sahiwal, Sahiwal, Pakistan*

ARTICLE INFO

Article History:
Received 10 April 2025
Accepted 25 June 2025
Published 01 July 2025

Keywords:
Hydrogel
Nanocomposite
Titanium dioxide
Pb (II) ions
Water treatment

ABSTRACT

The increasing contamination of water bodies by heavy metals, particularly lead (Pb (II)), poses a significant threat to environmental and public health. This research investigates the synthesis, characterization, and Pb (II) adsorption capabilities of a novel sodium alginate-g-poly (acrylic acid-co-Itaconic acid)/ titanium dioxide [SA-g-p(AA-IA)/ TiO_2] hydrogel nanocomposite. The nanocomposite was synthesized via free-radical polymerization and characterized using FTIR, XRD, and FESEM, which confirmed successful grafting, the incorporation of TiO_2 nanoparticles, and a porous structure. The influence of various operational parameters, including time, pH, temperature, and Pb (II) dose, on adsorption was systematically evaluated. The nanocomposite demonstrated a substantial Pb (II) adsorption capacity, reaching approximately 998.62 mg/g at pH 10, with equilibrium attained within 90 minutes. Kinetic analysis indicated that adsorption followed a pseudo-second model, suggesting chemisorption as primary mechanism. Adsorption isotherm data fitted to Freundlich and Temkin models, showing multilayer adsorption. Thermodynamic analysis revealed the process to be spontaneous (ΔG = -5.439 kJ/mol) and endothermic (ΔH = 23.404 kJ/mol). The hydrogel composite also exhibited pH-sensitive swelling behavior, with maximum swelling observed under alkaline conditions. These results highlight potential of SA-g-p(AA-IA)/ TiO_2 nanocomposite as an effective adsorbent for Pb (II) removal from solutions.

How to cite this article
Mutashar M., Shahad R., Jasim L., Batool M. Removal of Pb (II) Ions from Water by Adsorption on Sodium Alginate-g-poly (Acrylic acid-co-Itaconic acid)/Titanium Dioxide [SA-g-p(AA-IA)/ TiO_2] Hydrogel Nanocomposite . J Nanostruct, 2025; 15(3):983-996. DOI: 10.22052/JNS.2025.03.016

INTRODUCTION

The enduring presence of organic and inorganic pollutants, particularly heavy metals lead to polluting air, soil, and water [1]. Non-biodegradable pollutants like heavy metals can accumulate in living organisms through the food chain, drinking water, and air [2, 3], posing risks to human health, aquatic life, and the overall ecosystem [4, 5]. Water, a vital natural resource, is increasingly affected by the industrial release

* *Corresponding Author Email: layth.alhayder@gmail.com*

of chemicals, especially heavy metals [5]. Among various heavy metals, lead stands out due to its severe toxicity. It can lead to kidney problems, destroy red blood cells, damage the central nervous system, and ultimately cause death [6-12]. Therefore, addressing and eliminating such heavy metal pollution is crucial. Adsorption stands out as a highly favored and widely researched method for eliminating heavy metals from wastewater due to its operational simplicity, high removal efficiency even at low pollutant concentrations, cost-effectiveness, and the possibility of adsorbent regeneration and reuse, supporting sustainability [13-15]. The process relies on the transfer of adsorbate from liquid to surface of a solid adsorbent, where they are held by various physical and chemical interactions [16, 17]. These interactions encompass electrostatic forces, van der Waals forces, hydrogen bonding, and potentially chemical bond formation. Consequently, current research heavily emphasizes the synthesis of new adsorbents with optimized properties to maximize metal i.e., Pb (II) removal, including exploring different materials, refining their synthesis, and modifying their surface characteristics to enhance their affinity for Pb (II) removal [18, 19].

Hydrogels, capable of significant swelling in water, can be synthesized from various natural polysaccharides like sodium alginate (SA), chitosan, cellulose, starch, gellan gum, and guar gum, as well as synthetic polymers as poly (acrylic acid) (AA), poly (Itaconic acid) (IA), and poly (N-vinyl pyrrolidone) (PNVP) [20, 21]. Polysaccharide-based hydrogels are especially appealing for environmental cleanup due to their biocompatibility, biodegradability, low cost, and natural availability and sustainable development principles [22-25]. Their swelling ability generates a large network structure with extensive surface contact, promoting pollutant molecule diffusion and enhancing adsorption. Moreover, their chemical and physical properties can be precisely controlled during synthesis to introduce specific functional groups with high affinity for particular pollutant types, enabling the synthesis of selective and efficient adsorbents [26]. Current research focuses on advanced synthesis techniques like graft copolymerization, interpenetrating polymer networks, and nanomaterial incorporation to improve mechanical strength and adsorption capacity, aiming to develop more effective hydrogel adsorbents for practical wastewater treatment [27].

This study centers on synthesis and application of SA-g-p(AA-IA)/TiO_2 nanocomposite hydrogel to harness synergistic benefits of a natural polysaccharide (SA), synthetic monomers (AA and IA), and inorganic nanoparticles (TiO_2) for removal of (Pb (II)) ions from solutions [28]. Sodium alginate, an anionic polysaccharide derived from seaweed, is a readily available, cost-effective, and biodegradable biopolymer providing a biocompatible matrix for hydrogel formation [29]. Grafting acrylic acid onto alginate backbone introduces pH-responsive carboxylic acid functional groups, which enhance adsorption of cationic metal ions like Pb (II), particularly under alkaline conditions [30]. The incorporation of Itaconic acid, a non-ionic monomer, into polymer network contributes to hydrogel's overall structural integrity, mechanical strength, and water swelling capacity, facilitating accessibility of adsorption sites within hydrogel matrix [31]. The inclusion of TiO_2 nanoparticles within hydrogel matrix introduces a component known for its high surface area and potential interactions with metal ions [32, 33].

The specific objectives of this research include: i. Synthesizing and thoroughly characterizing the SA-g-p(AA-IA)/TiO_2 hydrogel nanocomposite using appropriate analytical techniques to confirm its successful formation and to understand its structural and morphological properties. ii. Systematically evaluating the influence of key operational parameters, as time, pH of solution, temperature and Pb (II) concentration on efficiency of process. iii. Determining the adsorption kinetics by applying established kinetic models, including pseudo-first-order and pseudo-second-order models, to experimental data obtained under various conditions to elucidate the rate-controlling steps and mechanism of adsorption. iv. Calculating the thermodynamic parameters, as Gibbs free energy change (ΔG), enthalpy change (ΔH), and entropy change (ΔS), to assess spontaneity of adsorption process and to determine whether it is endothermic or exothermic in nature. v. Analyzing the adsorption equilibrium data using various isotherm models as Langmuir, Freundlich, and Temkin models, to determine maximum adsorption capacity of nanocomposite for Pb (II) ions and to gain insights into nature of adsorption mechanism at solid-liquid interface. A comprehensive investigation of isothermal,

kinetics, and thermodynamics of Pb (II) removal on SA-g-p(AA-IA)/ TiO_2 will provide a thorough understanding of adsorption mechanism, enabling the optimization of its performance for efficient and sustainable removal of this heavy metal from wastewater.

MATERIALS AND METHODS

Chemicals used

This study employed a range of chemical reagents sourced from various suppliers, each with specific purities. Sodium alginate with a purity of 99.0% was obtained from Himedia. Titanium dioxide with 99.7% purity was supplied by Merck. Itaconic acid at 99% purity and N,N'-methylene-bis-acrylamide at 99% purity were both acquired from Himedia Laboratories. Potassium persulfate with 99% purity was purchased from Riedel-dehaenag seclze hannover. Ethanol with a purity of 95% was obtained from Merck ENERGY, while acrylic acid at 99% purity was from Himedia. Nitrogen gas was supplied by Xinrui. Sodium hydroxide with 99% purity was acquired from Alpha Chemika, and hydrochloric acid with a concentration of 38% was from J.T. Baker. Calcium carbonate with 99% purity, potassium chloride with 99.5% purity, and tetramethylethylenediamine with 99.0% purity were all sourced from Fluka. Additionally, lead nitrate with 99.0% purity was obtained from Himedia Laboratories.

Synthesis of SA-g-p(AA-IA)/ TiO_2 Nanocomposite Hydrogel

The SA-g-p(AA-IA)/ TiO_2 underwent synthesis via free-radical copolymerization in an aqueous environment. The process commenced with the dispersion of 0.12 g of TiO_2 nanoparticles in 20 mL of deionized water, achieved through 4 hours of continuous stirring followed by an additional 4 hours of ultrasonication. This dispersion was then transferred to a three-necked round-bottom flask fitted with a condenser, a dropping funnel, and a nitrogen gas inlet, and placed in a stirred water bath until complete dissolution was observed. Subsequently, 0.5 g of sodium alginate (SA) was introduced into the reaction mixture and agitated for 1 hour to yield a homogeneous solution. Next, 4 g of acrylic acid (AA) added dropwise to preceding solution under continuous stirring for 15 minutes. Following this, a solution prepared by dissolving 2 g of Itaconic acid (IA) in 2 mL of H_2O until fully dissolved was added gradually to the reaction mixture over 15 minutes of constant stirring. In a similar manner, 0.05 g of N, N'-methylenebisacrylamide (MBA) as a cross-linking agent was dissolved in 2 mL of H_2O and added slowly to the solution with 15 minutes of agitation.

Batch adsorption and calibration curve

To assess the synthesized SA-g-p(AA-IA)/TiO_2 capacity as an adsorbent for removing Pb (II) ions from water, batch experiments were conducted. The parameters investigated for Pb (II) adsorption included contact time (0-300 min), temperature (10, 15, 20, 30 °C), initial Pb (II) concentration (100-500 mg/L) and pH (2-10). Each experiment involved agitating 10 mL of Pb (II) solution in a conical flask at a shaking speed of 130 rpm. The pH of the solutions was adjusted using 0.1 M NaOH and HCl solutions, and a pH meter was used for measurement. Following the attainment of equilibrium, the concentration of Pb (II) remaining in the solution was determined using an atomic absorption spectrophotometer (AAS) at its characteristic wavelength. Subsequently, the quantity of Pb (II) adsorbed per unit mass of the adsorbent (mg/g) and the percentage removal of Pb (II) were calculated by Eqs. 1 and 2 correspondingly [34].

$$q_e = \frac{C_o - C_e * V}{m} \quad (1)$$

$$R\,(\%) = \frac{C_o - C_e}{C_o} \text{ x}100 \quad (2)$$

here, and refers to initial and equilibrium concentrations of Pb (II) solution (mg/L), correspondingly while "m" denotes dose of nanocomposite (g) and volume of pollutant solution used is represented by V (L).

A calibration curve for Pb (II) ions (**Fig. 1**) was established by measuring the absorbance of standard Pb (II) solutions at its characteristic wavelength using AAS. This curve demonstrated a strong linear correlation between absorbance and concentration, consistent with Beer-Lambert's law. The resulting linear equation with a high coefficient of determination (R^2 = 0.998) provided a reliable method for quantifying Pb (II) concentrations in adsorption studies, enabling calculation of residual Pb (II) concentration, adsorption capacity, and Pb (II) removal efficiency.

RESULTS AND DISCUSSION

Characterization analysis

Examining the SA-g-p(AA-IA)/ TiO_2 nanocomposite using FTIR spectroscopy before and after Pb (II) ion adsorption reveals significant modifications in characteristic peaks of functional groups. The initial FTIR spectrum of nanocomposite (Fig. 2), prior to Pb (II) exposure,

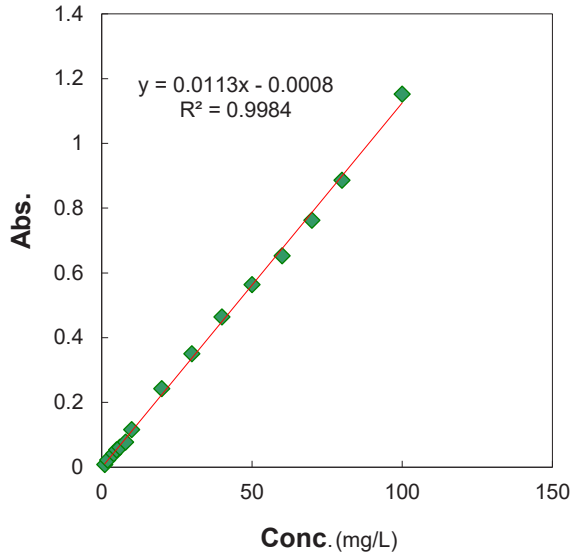

Fig. 1. Calibration plot for Pb (II) ion solution.

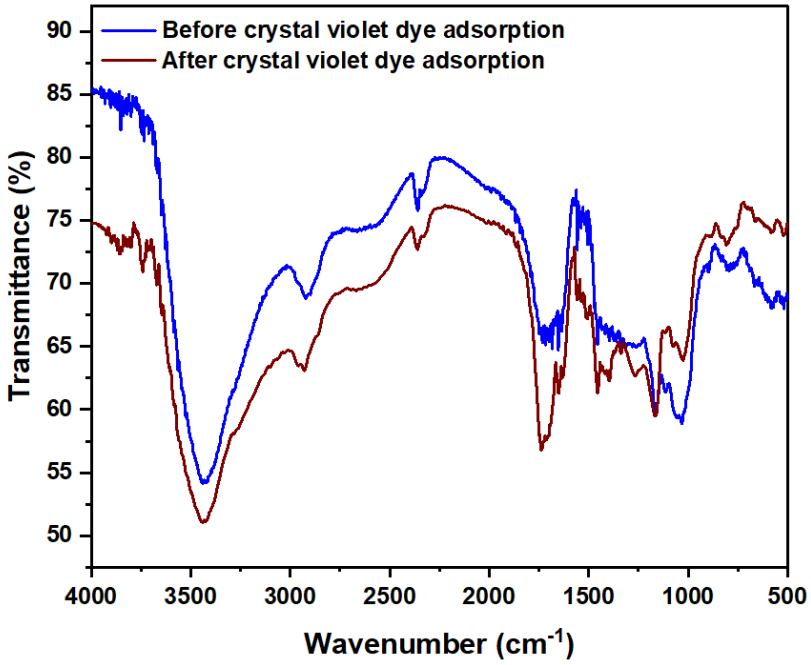

Fig. 2. FTIR of nanocomposite before and after Pb (II) ions adsorption.

displayed peaks corresponding to functional groups of its constituent components: sodium alginate (SA), acrylic acid (AA), Itaconic acid (IA), and TiO_2. A broad absorption band observed in range of 3300–3400 cm^{-1} indicated the presence of stretching vibrations of –OH and –NH bonds, originating from hydroxyl groups of alginate and the amide groups of IA. A prominent peak around 1650 cm^{-1} was attributed to C=O stretching vibration within amide I groups. A band appearing between 1550–1600 cm^{-1} likely represented N–H bending (amide II) or asymmetric stretching of carboxylate ($–COO^-$) ions from AA. The symmetric stretching of $–COO^-$ groups appeared in region of 1400–1450 cm^{-1}. Furthermore, a strong band around 1020–1080 cm^{-1} corresponds to C–O–C stretching. Further, TiO_2 was confirmed by a band in the range of 500–700 cm^{-1} of spectra. Following the adsorption of Pb (II) ions, the FTIR spectrum displayed noticeable shifts and changes in intensity of several peaks, suggesting interactions between metal ions and functional groups of composite. The –OH/ –NH stretching band became broader and underwent a slight shift in wavenumber, indicating the potential formation of coordination bonds or electrostatic interactions between the Pb (II) ions and composite's polar groups. The peak at 1650 cm^{-1} (C=O stretching) exhibited a minor shift and a decrease in intensity, implying an interaction between Pb (II) and amide or carboxylic acid functionalities. Furthermore, the peak near 1550 cm^{-1} showed a shift or a change in intensity, which is attributed to involvement of carboxylate or amine groups in ionic binding with Pb (II) ions. Variations observed in 1400–1450 cm^{-1} region suggested possible interactions between positive charges of Pb (II) and carboxyl groups of nanocomposite, potentially through ionic exchange or complexation. The C–O–C peak near 1020–1080 cm^{-1} might have also experienced a change in intensity due to minor rearrangements in polymer backbone upon Pb (II) adsorption [35-38].

XRD analysis revealed the crystalline nature of pure TiO_2 nanoparticles, with sharp peaks corresponding to anatase phase, as evidenced in Fig. 3a. Upon incorporation of TiO_2 into SA-g-p(AA-IA) hydrogel, the resulting nanocomposite (Fig. 3b) exhibited significantly weaker and broader TiO_2 peaks, indicating a reduction in crystallite size and distortion of TiO_2 structure due to dispersion within amorphous polymer network. The presence of a broad halo between 15° and 30° in nanocomposite XRD pattern confirmed non-crystalline nature of hydrogel matrix, while persistence of characteristic anatase TiO_2 peaks, even though with reduced intensity, suggested that the TiO_2 nanoparticles retained their crystalline structure within composite material [39].

FESEM images of nanocomposite prior to Pb (II) ion adsorption (Fig. 4a, 10 µm scale) revealed a textured, porous surface with numerous irregularities and openings, indicative of a substantial surface area potentially beneficial for metal ion adsorption. The TiO_2 nanoparticles appeared distributed throughout hydrogel

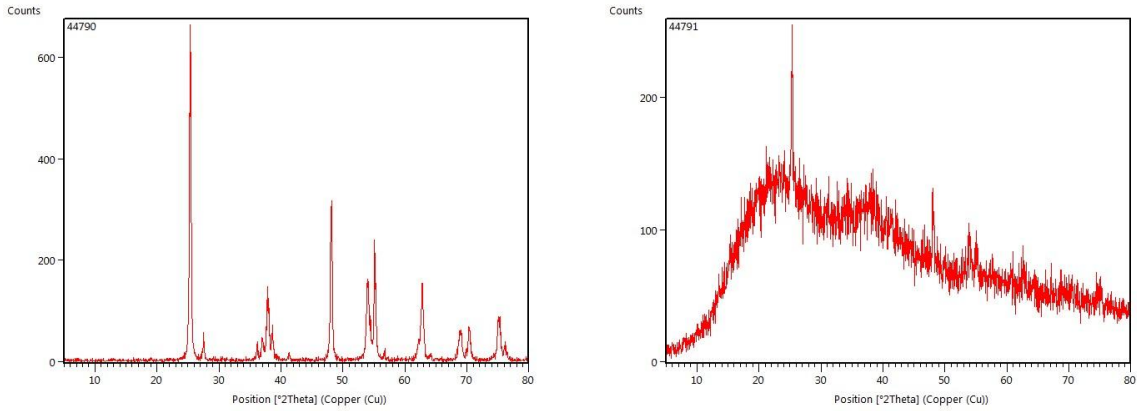

(a) **(b)**

Fig. 3. XRD of (a) TiO_2 and (b) SA-g-p(AA-IA)/ TiO_2 nanocomposite.

matrix, which could contribute to the material's mechanical stability and enhance its affinity for Pb (II) ions via surface interactions. In contrast, FESEM image of nanocomposite following Pb (II) ion adsorption (Fig. 4b, 5 µm scale) displayed a considerably smoother and more compact surface morphology. The previously observed pores and openings appeared to be filled or covered, suggesting that Pb (II) ions had successfully bound to and permeated the nanocomposite's surface. This transformation from a porous to a smoother texture provided visual confirmation of material's adsorptive capabilities for Pb (II) ions [38].

Kinetic study

The influence of time on adsorption of Pb

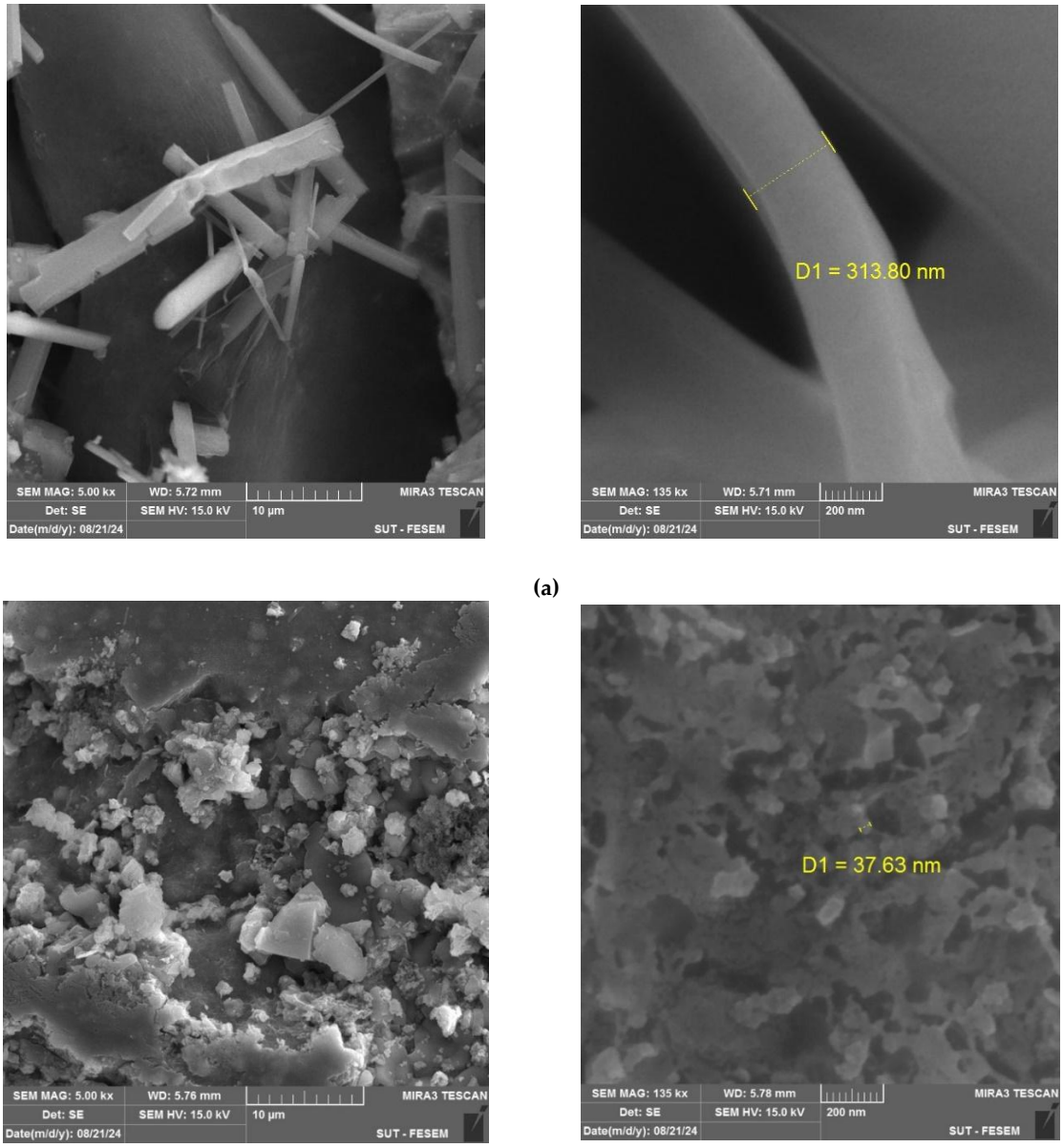

Fig. 4. FESEM of SA-g-p(AA-IA)/ TiO_2 (a) before and (b) after Pb (II) ions adsorption.

(II) ions by nanocomposite (Fig. 5a-b) was evaluated by examining the adsorption capacity (Q_e) and percentage removal (% RE). The results demonstrated a rapid initial phase of Pb (II) uptake. Within the first minute, a Q_e of 815.31 mg/g and a %RE of 65.22% were observed, indicating a fast initial binding of Pb (II) ions to readily available active sites on nanocomposite surface. This was followed by a substantial increase within the initial 15 minutes, reaching a Q_e of 1093.78 mg/g and a %RE of 87.50%, highlighting a strong initial mass transfer driven by concentration gradient and availability of active sites. Subsequently, the adsorption rate decreased in an intermediate phase (15-90 minutes) as these active sites became progressively occupied. Eventually, system approached equilibrium in later stages (beyond 90 minutes), with minimal further change observed in Q_e and %RE, suggesting that adsorption saturation was largely achieved by 90 minutes. The maximum Q_e reached at equilibrium was approximately 1237.66 mg/g, with a corresponding %RE of around 99.01%. This indicates that a contact time of 90 minutes was sufficient for nanocomposite to effectively adsorb Pb(II) ions under studied conditions [40].

To gain insight into the mechanism and rate-controlling step of Pb (II) ion adsorption onto nanocomposite hydrogel over time, pseudo-first-order and pseudo-second-order kinetic models were employed. The pseudo-first-order model posits that rate of adsorption site occupancy is proportional to number of unoccupied sites, while pseudo-second-order model suggests that rate-limiting step involves chemisorption, characterized by sharing of electrons between adsorbent and adsorbate (Pb (II) ions). Eqs. 3 and 4 represent mathematical expressions for pseudo-first-order and pseudo-second-order models, correspondingly:

$$\log(Q_e - Q_t) = \log Q_e - \frac{k_1}{2.303} t \quad (3)$$

$$\frac{t}{Q_t} = \frac{1}{k_2 Q_e^2} + \frac{t}{Q_e} \quad (4)$$

here, q_t and q_e refers to amounts of adsorbate adsorbed at time t and at equilibrium, respectively (mg/g) while k_1 and k_2 refers pseudo-first rate constant (min^{-1}) and second order model (g/mg·min), correspondingly. The kinetic study results (Fig. 6a-b and Table 1) indicated that pseudo-first-order model did not effectively represent adsorption of Pb (II) ions by nanocomposite, as evidenced by its lower regression coefficient compared to pseudo-second model. This suggests

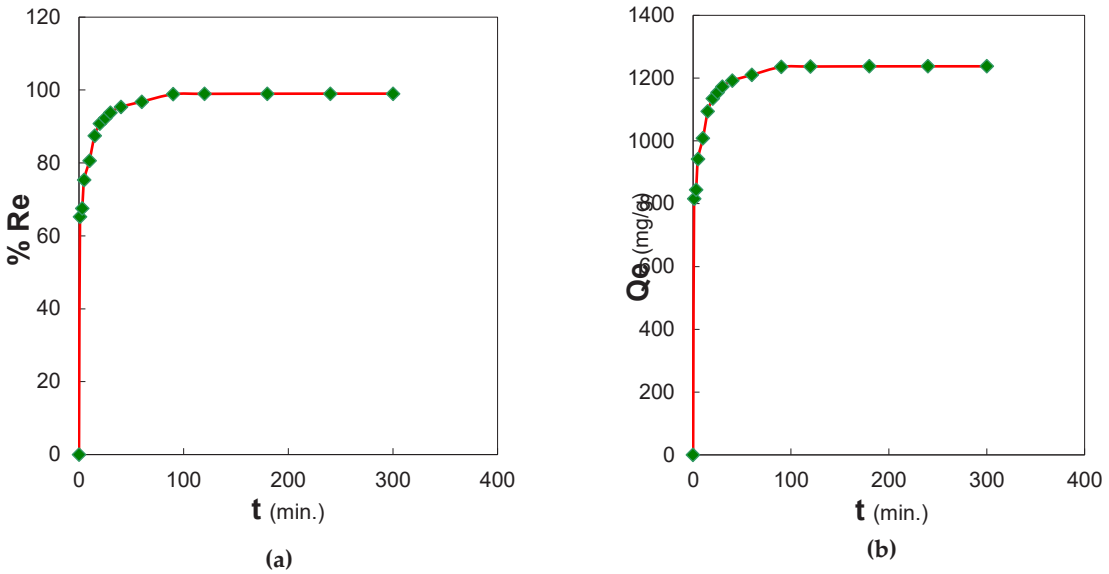

Fig. 5. Effect of time on (a) % removal and (b) Q_e, mg/g, for Pb (II) adsorption.

that the adsorption process is not solely governed by physical diffusion. Conversely, pseudo-second model provided a better fit to kinetic data, implying that chemisorption is the predominant mechanism. This likely involves interactions as electrostatic forces or complexation between Pb (II) ions and functional groups (e.g., –COOH, –NH_2) present on nanocomposite [41].

Isothermal and temperature study

The adsorption capacity (Q_e) of nanocomposite for Pb (II) ions was observed to increase with higher initial Pb (II) concentrations across all tested temperatures (10, 15, 20, and 30 °C) (Fig. 7). Specifically, at 10 °C, Q_e values were 249.82 mg/g at an initial Pb (II) concentration (C_o) of 100 mg/L, 374.16 mg/g at 150 mg/L, and 1024.16 mg/g at 500 mg/L. Similar trends were observed at 15 °C (Q_e values of 249.82, 374.82, and 1081.68 mg/g for C_o of 100, 150, and 500 mg/L, respectively), 20 °C (Q_e values of 249.82, 374.82, and 1102.26 mg/g for Co of 100, 150, and 500 mg/L, respectively), and 30 °C (Qe values of 249.82, 374.82, and 1125.93 mg/g for C_o of 100, 150, and 500 mg/L, respectively). These results indicate that a higher availability of Pb (II) ions in solution, resulting from increased concentrations, provides a greater driving force for Pb (II) ions towards adsorbent surface and their subsequent binding. Furthermore, the effect of temperature on adsorption capacity appears to be complex. While there is a slight increase in Q_e with rising temperature from 10 °C to 30 °C at higher initial Pb (II) concentrations (e.g., C_o of 500 mg/L), the adsorption capacity at lower concentrations

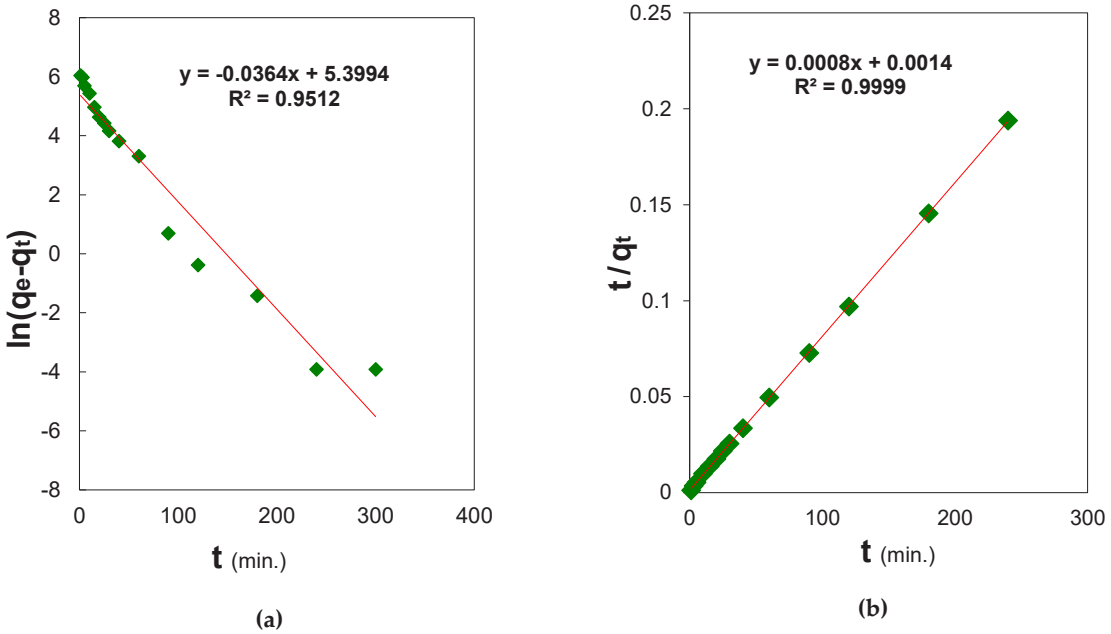

Fig. 6. Plot for (a) pseudo first and (b) pseudo second model.

Table 1. Pseudo first and second model parameters. Experimental (mg/g) = 1237.6 mg/g.

Model	Pseudo-first order	Pseudo-second order
q_e (mg/g)	221.2	1250
R^2 values	0.951	0.999
Constant	0.0364	0.0004
	$K_1(1/\text{min})$	$K_2\,(\text{g/mg}\cdot\text{min})$

(e.g., C_o of 100 and 150 mg/L) remains relatively consistent across tested temperature range [39, 42, 43].

Thermodynamic parameters such as Gibbs free energy change (ΔG), enthalpy change (ΔH), and entropy change (ΔS) offer essential information

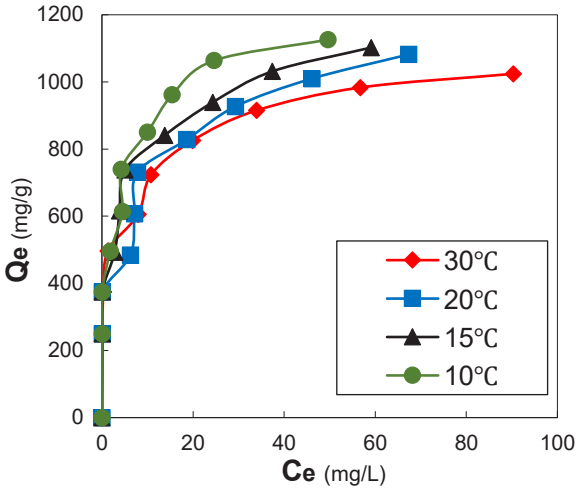

Fig. 7. Effect of Pb (II) concentration at different temperatures.

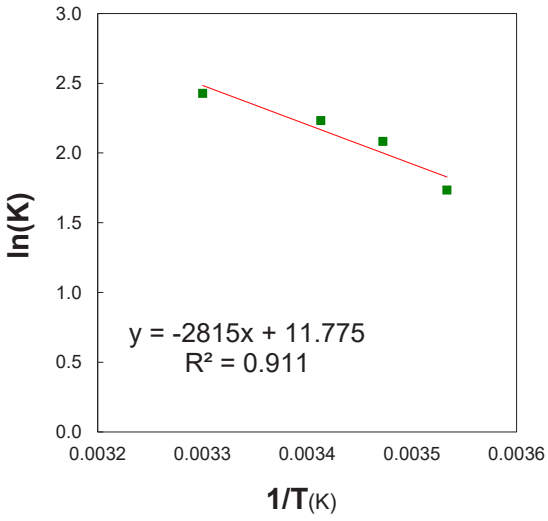

Fig. 8. Van't Hoff plot.

Table 2. Thermodynamic parameters.

T (°C)	ΔG (kJ/mol)	ΔH (kJ/mol)	ΔS (J/mol K)	K_c
20	-5.439	23.404	97.897	9.326

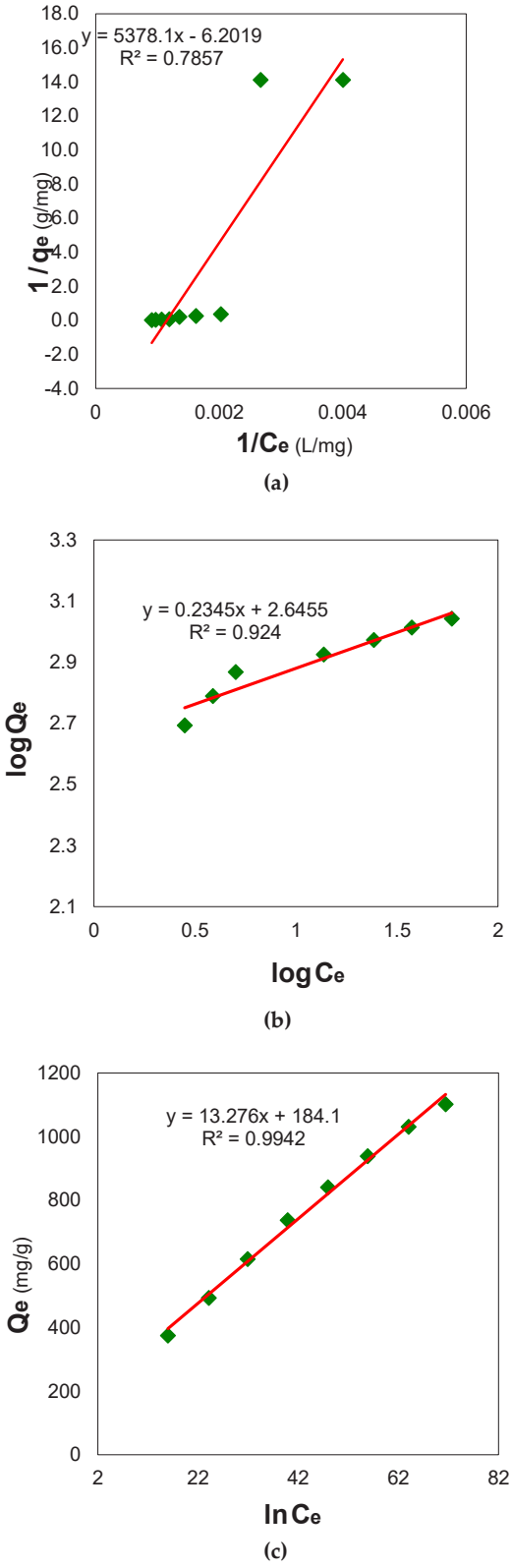

Fig. 9. Graphs for (a) Langmuir, (b) Freundlich and (c) Temkin models.

regarding feasibility and spontaneity of adsorption process, as well as changes in order or disorder at solid-solution interface. Utilizing data obtained at 20 °C (from the Van't Hoff plot, Fig. 8), the thermodynamic parameters for Pb (II) adsorption were determined (Table 2). These values include a ΔG of -5.439 kJ/mol, indicating that the adsorption of Pb (II) ions onto nanocomposite is a spontaneous process under these conditions. Furthermore, the ΔH value of 23.404 kJ/mol reveals that adsorption process releases heat, and is therefore exothermic. Additionally, ΔS value of 97.897 J/mol·K suggests feasibility of process. This reduction in randomness is likely attributed to ordering of Pb (II) ions as they become immobilized on specific sites of adsorbent surface, resulting in a decrease in their degrees of freedom compared to their state in the aqueous solution [44].

To better understand the mechanisms governing the interaction between Pb (II) ions and nanocomposite surface, three adsorption isotherm models were applied: Langmuir, Freundlich, and Temkin isotherms. The Langmuir model (Eq. 5) operates on assumptions of monolayer adsorption, where a single layer of adsorbate ions forms on a uniform adsorbent surface with a limited number of identical adsorption sites. The Freundlich isotherm (Eq. 6) describes multilayer adsorption on heterogeneous surfaces, where enthalpy of adsorption changes with extent of surface coverage. In contrast, the Temkin model (Eq. 7) considers interactions between adsorbed ions and assumes that enthalpy of adsorption decreases linearly with surface coverage.

$$\frac{1}{q_e} = \frac{1}{q_{max}} + \frac{1}{q_o b C_e} \quad (5)$$

$$\log q_e = \log K_f + \frac{1}{n}\log C_e \quad (6)$$

$$q_{eq} = B\ln A_T + B\ln C_{eq} \quad (7)$$

where, q_e is equilibrium adsorption capacity, q_{max} is maximum adsorption capacity, K_L is Langmuir constant, Ce is equilibrium adsorbate concentration, K_f is Freundlich constant, 1/n is an empirical parameter of surface heterogeneity, R is gas constant, T is absolute temperature, b is Temkin constant related to heat of adsorption, and A is Temkin isotherm constant. Isotherm analysis (Fig. 9a-c) indicated that the adsorption behavior of Pb (II) ions onto nanocomposite could be effectively described by both Freundlich and Temkin models, as evidenced by their high R^2 values. This suggests that the composite surface likely presents

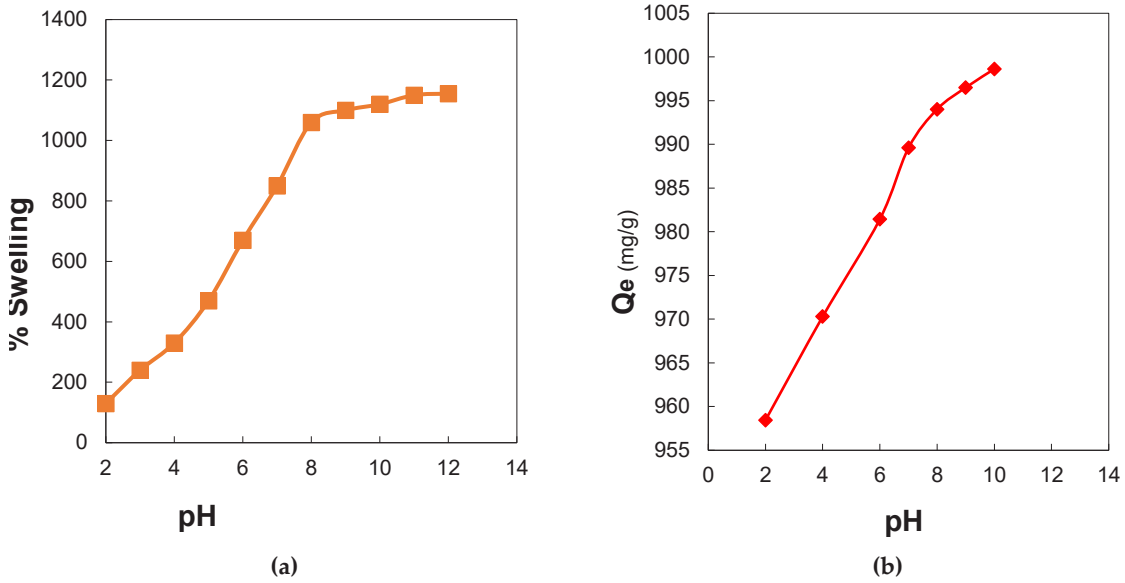

(a) (b)

Fig. 10. Effect of pH on (a) swelling ratio and (b) adsorption capacity of nanocomposite for Pb (II) ions.

energetically diverse sites, facilitating multilayer adsorption characterized by varying adsorption energies and interactions between adsorbed Pb (II) ions [45].

Effect of pH

he swelling behavior of the SA-g-p(AA-IA)/TiO_2 nanocomposite hydrogel is markedly dependent on pH, as surrounding ionic conditions influence charge of functional groups within its polymeric framework, and this is quantified by Eq. 8:

$$\text{Swelling ratio } (\%) = \frac{W_S - W_d}{W_d} \times 100 \quad (8)$$

Under acidic conditions (Fig. 10a), the hydrogel exhibited limited swelling. At pH 2, the swelling percentage was 130%, gradually increasing to 240% at pH 3 and 330% at pH 4. This constrained swelling in acidic environments is primarily due to the protonation of carboxylic (–COOH) and amide groups, which reduces the repulsive forces between the polymer chains and limits the hydrogel's water uptake capacity. As the pH increased to 5 and beyond, a significant enhancement in swelling capacity was observed. At pH 5, the swelling percentage reached 470%, continuing to rise substantially to 670% at pH 6, 850% at pH 7, and reaching a high of 1060% at pH 8. This considerable increase is attributed to the deprotonation of –COOH groups, forming $–COO^-$ ions, which leads to stronger electrostatic repulsion within the polymer network. The increased density of negative charges causes the hydrogel structure to expand more extensively, enabling greater water absorption. Beyond pH 8, the swelling capacity continued to increase, but at a slower pace, reaching 1100% at pH 9, 1120% at pH 10, and eventually plateauing at 1155% at pH 12. This leveling off indicates that ionizable groups within polymer have largely lost their protons, and hydrogel structure has approached its maximum expansion in alkaline conditions [46].

The adsorption capacity (Q_e) of nanocomposite for Pb (II) ions was significantly influenced by pH of solution (Fig. 10b). At a highly acidic pH of 2, Q_e was 958.44 mg/g. This relatively high adsorption under acidic conditions suggests a strong interaction between Pb (II) ions and protonated functional groups on adsorbent surface. As pH increased to 4 and then to 6, adsorption capacity showed a slight improvement, reaching 970.30 mg/g and 981.45 mg/g, respectively. This increase indicates that as concentration of H^+ ions decreased, more favorable binding sites for Pb (II) ions became available. A further increase in adsorption was observed at pH 7 and 8, where Q_e values were 989.59 mg/g and 994.02 mg/g, respectively, suggesting that near-neutral to slightly alkaline conditions are optimal for Pb (II) adsorption onto this nanocomposite. Further increases in pH to 9 and 10 resulted in a minimal additional increase in adsorption capacity to 996.50 mg/g and a peak of 998.62 mg/g, indicating that a weakly basic pH provides the most effective adsorption of Pb (II) ions. These results highlight pH-dependent surface charge of nanocomposite and its impact on electrostatic interactions with Pb (II) ions [46].

CONCLUSION

In this study, a SA-g-p(AA-IA)/ TiO_2 hydrogel nanocomposite was successfully synthesized and its effectiveness in removing Pb (II) ions from aqueous solutions was evaluated. The material exhibited favorable structural and surface properties, as confirmed by FTIR, XRD, and FESEM analyses, which supported its strong affinity for Pb (II). The adsorption was significantly influenced by operational factors, particularly pH, where weakly basic conditions enhanced adsorption. Kinetic modeling indicated that adsorption process followed pseudo-second-order kinetics, suggesting a chemical adsorption mechanism. Isotherm analysis revealed that adsorption behavior was best described by both Freundlich and Temkin models, indicating multilayer adsorption on a heterogeneous surface. The thermodynamic parameters confirmed spontaneity and exothermic nature of adsorption process. The composite also demonstrated pH-sensitive swelling behavior, with high adsorption capacity achieved under specific conditions. These findings suggest that the SA-g-p(AA-IA)/ TiO_2 hydrogel nanocomposite shows promise as an efficient adsorbent for removal of Pb (II) ions from contaminated water.

CONFLICT OF INTEREST

The authors declare that there is no conflict of interests regarding the publication of this manuscript.

REFERENCES

1. Kaur M, Kumari S, Sharma P. Removal of Pb (II) from

aqueous solution using nanoadsorbent of Oryza sativa husk: Isotherm, kinetic and thermodynamic studies. Biotechnology reports (Amsterdam, Netherlands). 2019;25:e00410-e00410.
2. Shah A, Zakharova J, Batool M, Coley MP, Arjunan A, Hawkins AJ, et al. Removal of cadmium and zinc from water using sewage sludge-derived biochar. Sustainable Chemistry for the Environment. 2024;6:100118.
3. Kariuki Z, Kiptoo J, Onyancha D. Biosorption studies of lead and copper using rogers mushroom biomass ' Lepiota hystrix '. South African Journal of Chemical Engineering. 2017;23:62-70.
4. Benila Smily JRM, Sumithra PA. Optimization of Chromium Biosorption by Fungal Adsorbent, Trichoderma sp. BSCR02 and its Desorption Studies. HAYATI Journal of Biosciences. 2017;24(2):65-71.
5. Saravanan R, Gupta VK, Narayanan V, Stephen A. Visible light degradation of textile effluent using novel catalyst ZnO/γ-Mn2O3. Journal of the Taiwan Institute of Chemical Engineers. 2014;45(4):1910-1917.
6. Amro AN, Abhary MK. Removal of lead and copper ions from water using powdered Zygophyllum coccineum biomass. International Journal of Phytoremediation. 2019;21(14):1457-1462.
7. Qu X, Alvarez PJJ, Li Q. Applications of nanotechnology in water and wastewater treatment. Water Res. 2013;47(12):3931-3946.
8. Kataria N, Garg VK. Optimization of Pb (II) and Cd (II) adsorption onto ZnO nanoflowers using central composite design: isotherms and kinetics modelling. J Mol Liq. 2018;271:228-239.
9. Hmood NA, Mother Othman DMA, Mohsin Ali DM. Transcription Factor 7-Like 2 Gene Polymorphisms rs7903146associationwith Type 2 Diabetic Polycystic Ovarian Syndrome Women of Iraqi Population. Annals of Tropical Medicine and Public Health. 2019;22(12):156-164.
10. Dehghani Ghorbi M, Jasim Qasim M, H Kadhum AA, Abdul-Mounther Othman M, Dehghani A, Ghaffariyan S, et al. An ecological assessment of global thyroid cancer incidence and mortality according to the human development index in 2020. Journal of Parathyroid Disease. 2025;13:e12275.
11. Ali MM, Mhaibes RM, Othman MA-M, R. Lahhob Q, Qasim MJ. Association between triglyceride-glucose index and risk of chronic kidney disease: a systematic review and meta-analysis. Journal of Nephropharmacology. 2024;13(2):e12692.
12. Al-Suraify SMT, Hussien LB. Synthesis and characterization of new compounds derived from 1H-indol-5-ylamine. Applied Nanoscience. 2022;13(3):2083-2092.
13. Majeed HJ, Idrees TJ, Mahdi MA, Abed MJ, Batool M, Yousefi SR, et al. Synthesis and application of novel sodium carboxy methyl cellulose-g-poly acrylic acid carbon dots hydrogel nanocomposite (NaCMC-g-PAAc/ CDs) for adsorptive removal of malachite green dye. Desalination and Water Treatment. 2024;320:100822.
14. Javed T, Thumma A, Uddin AN, Akhter R, Babar Taj M, Zafar S, et al. Batch adsorption study of Congo Red dye using unmodified Azadirachta indica leaves: isotherms and kinetics. Water Practice and Technology. 2024;19(2):546-566.
15. Sharma S, Sharma G, Kumar A, AlGarni TS, Naushad M, Alothman ZA, et al. Adsorption of cationic dyes onto carrageenan and itaconic acid-based superabsorbent hydrogel: Synthesis, characterization and isotherm analysis. J Hazard Mater. 2022;421:126729.
16. Shah A, Arjunan A, Thumma A, Zakharova J, Bolarinwa T, Devi S, et al. Adsorptive removal of arsenic from drinking water using KOH-modified sewage sludge-derived biochar. Cleaner Water. 2024;2:100022.
17. Jamel HO, Jasim MH, Mahdi MA, Ganduh SH, Batool M, Jasim LS, et al. Adsorption of Rhodamine B dye from solution using 3-((1-(4-((1H-benzo[d]imidazol-2-yl)amino) phenyl)ethylidene)amino)phenol (BIAPEHB)/ P(AA-co-AM) composite. Desalination and Water Treatment. 2025;321:101019.
18. Salunkhe B, Schuman TP. Super-Adsorbent Hydrogels for Removal of Methylene Blue from Aqueous Solution: Dye Adsorption Isotherms, Kinetics, and Thermodynamic Properties. Macromol. 2021;1(4):256-275.
19. Al-Asadi ST, Al-Qaim FF. Adsorption of Methylene Blue Dye from aqueous solution using low cost adsorbent: Kinetic, Isotherm Adsorption and Thermodynamic Studies. Research Square Platform LLC; 2023.
20. Van Tran V, Park D, Lee Y-C. Hydrogel applications for adsorption of contaminants in water and wastewater treatment. Environmental Science and Pollution Research. 2018;25(25):24569-24599.
21. Shahad RF. Studying the Effect of Agriculturally Exploited Soils on the Transformation of Mica Minerals using Infrared Spectroscopy (IR). Malaysian Journal of Chemistry. 2021;23(4).
22. Ogundiran AA, Ogundiran OO, Badeji AA, Osinubi AD. Kinetic, Isotherm And Thermodynamic Studies Of The Adsorption Of Cresol Red Dye Using Agricultural Wastes. Nigerian Journal of Science and Environment. 2024;22(2):28-50.
23. Mohammed Malik H, Raad Farhan S, Mohammad Tarkhan Abo A. Assessment of Groundwater Quality and Suitability for Irrigation Purpose in Northern Babil Governorate. Journal of Environmental and Earth Sciences. 2025;7(4):368-377.
24. Raad Farhan S, Mohammed Malik H. Impact of Bentonite and Humic Acid on the Growth and Flowering of Catharanthus roseus L. in Sandy Soil. Journal of Environmental and Earth Sciences. 2024;7(1):157-166.
25. Al-Zuhairy SH, Darweesh MA, Othman MA-M, Al-Zuhairy NA-HS. Vitamin D deficiency in young children with iron deficiency in Misan province, Iraq. J Med Life. 2022;15(3):387-391.
26. Nano Modifications of Biochar to Enhance Heavy Metal Adsorption from Wastewaters: A Review. American Chemical Society (ACS).
27. Sajeesh S, Sharma CP. Mucoadhesive hydrogel microparticles based on poly (methacrylic acid-vinyl pyrrolidone)-chitosan for oral drug delivery. Drug Deliv. 2010;18(4):227-235.
28. Abdul Sattar OD, Mohd Khalid R, M. Yusoff SF. Optimizing Methylene Blue Dye Adsorption onto Liquid Natural Rubber-Based Hydrogel: Kinetics, Isotherms and Reusability. Sains Malaysiana. 2024;53(5):1149-1166.
29. Aljeboree AM, Alkaim AF. Studying removal of anionic dye by prepared highly adsorbent surface hydrogel nanocomposite as an applicable for aqueous solution. Sci Rep. 2024;14(1):9102-9102.
30. Arshad R, Javed T, Thumma A. Exploring the efficiency of sodium alginate beads and Cedrus deodara sawdust for adsorptive removal of crystal violet dye. J Dispersion Sci Technol. 2023;45(12):2330-2343.
31. Guo H, Jiao T, Zhang Q, Guo W, Peng Q, Yan X. Preparation of Graphene Oxide-Based Hydrogels as Efficient Dye Adsorbents for Wastewater Treatment. Nanoscale research letters. 2015;10(1):931-931.
32. Aljeboree AM, Radia ND, Jasim LS, Alwarthan AA,

Khadhim MM, Washeel Salman A, et al. Synthesis of a new nanocomposite with the core TiO2/hydrogel: Brilliant green dye adsorption, isotherms, kinetics, and DFT studies. Journal of Industrial and Engineering Chemistry. 2022;109:475-485.
33. Lučić M, Milosavljević N, Radetić M, Šaponjić Z, Radoičić M, Kalagasidis Krušić M. The potential application of TiO2/hydrogel nanocomposite for removal of various textile azo dyes. Sep Purif Technol. 2014;122:206-216.
34. Javed T, Kausar F, Zawar MD, Khalid N, Thumma A, Ismail A, et al. Investigating the adsorption potential of coconut coir as an economical adsorbent for decontamination of lanthanum ion from aqueous solution. J Dispersion Sci Technol. 2024:1-12.
35. Pang YL, Tee SF, Limg S, Abdullah AZ, Ong HC, Wu C-H, et al. Enhancement of photocatalytic degradation of organic dyes using ZnO decorated on reduced graphene oxide (rGO). Desalination and Water Treatment. 2018;108:311-321.
36. Mannan HA, Nadeem R, Bibi S, Javed T, Javed I, Nazir A, et al. Mesoporous activated TiO_2 /based biochar synthesized from fish scales as a proficient adsorbent for deracination of heavy metals from industrial efflux. J Dispersion Sci Technol. 2022;45(2):329-341.
37. Faleh YA, Radhy ND. Removal of Metformin hydrochloride from Aqueous Solutions by using Carboxymethyl cellulose-g-poly(acrylic acid-co-acrylamide) Hydrogel: Adsorption and Thermodynamic Studies. IOP Conference Series: Earth and Environmental Science. 2021;790(1):012062.
38. Thakur S, Arotiba OA. Synthesis, swelling and adsorption studies of a pH-responsive sodium alginate–poly(acrylic acid) superabsorbent hydrogel. Polym Bull. 2018;75(10):4587-4606.
39. Marathe YV, Shrivastava VS. Effective removal of non-biodegradable methyl orange dye by using CdS/activated carbon nanocomposite as a photocatalyst. Desalination and Water Treatment. 2015;53(5):1316-1323.
40. Al-Asadi ST, Mussa ZH, Al-Qaim FF, Kamyab H, Al-Saedi HFS, Deyab IF, et al. A comprehensive review of methylene blue dye adsorption on activated carbon from edible fruit seeds: A case study on kinetics and adsorption models. Carbon Trends. 2025;20:100507.
41. Ge H, Wang J. Ear-like poly (acrylic acid)-activated carbon nanocomposite: A highly efficient adsorbent for removal of Cd(II) from aqueous solutions. Chemosphere. 2017;169:443-449.
42. Abdullah AR, Jasim LS. High-efficiency removal of diclofenac sodium (DS) drug using chitosan-grafted-poly(acrylic acid-co-N-isopropylacrylamide)/kaolin clay hydrogel composite. Int J Environ Anal Chem. 2024:1-21.
43. Atyaa AI, Jasim LS, Jamel HO, Sahib IJ. Adsorption of the crystal violet from aqueous solutions on (BIAPEHB/P(AA-co-AM)) composite: Thermodynamic study. AIP Conference Proceedings: AIP Publishing; 2023. p. 040139.
44. Batool M, Javed T, Wasim M, Zafar S, Din MI. Exploring the usability of Cedrus deodara sawdust for decontamination of wastewater containing crystal violet dye. Desalination and Water Treatment. 2021;224:433-448.
45. Bukhari A, Javed T, Haider MN. Adsorptive exclusion of crystal violet dye from wastewater by using fish scales as an adsorbent. J Dispersion Sci Technol. 2022;44(11):2081-2092.
46. Rafak SH, Jasim LS. Synthesis of novel bentonite/pectin-grafted-poly(crotonic acid-co-acrylic acid) hydrogel nanocomposite for adsorptive removal of safranin O dye from aqueous solution. Int J Environ Anal Chem. 2024:1-24.